Journal of Geophysical Research: Solid Earth

RESEARCH ARTICLE
10.1002/2017JB015206

Key Points:
- Fault slip and GPS velocities define a curved velocity field around the eastern Himalayan syntaxis
- Total geodetic slip rate across the sinistral-slip faults of the Shan Plateau is ~12 mm/year, consistent with geologic rates over 10 Ma
- The southwestward tongue-like pattern of slip rates across the Shan Plateau constrains regional geodynamic models

Supporting Information:
- Supporting Information S1

Correspondence to:
X. Shi,
xshi@ntu.edu.sg

Citation:
Shi, X., Wang, Y., Sieh, K., Weldon, R., Feng, L., Chan, C.-H., & Liu-Zeng, J. (2018). Fault slip and GPS velocities across the Shan Plateau define a curved southwestward crustal motion around the eastern Himalayan syntaxis. *Journal of Geophysical Research: Solid Earth*, *123*, 2502–2518. https://doi.org/10.1002/2017JB015206

Received 8 NOV 2017
Accepted 6 MAR 2018
Accepted article online 10 MAR 2018
Published online 30 MAR 2018

Fault Slip and GPS Velocities Across the Shan Plateau Define a Curved Southwestward Crustal Motion Around the Eastern Himalayan Syntaxis

Xuhua Shi[1], Yu Wang[1,2], Kerry Sieh[1], Ray Weldon[1,3], Lujia Feng[1], Chung-Han Chan[1], and Jing Liu-Zeng[4]

[1]Earth Observatory of Singapore, Nanyang Technological University, Singapore, [2]Department of Geosciences, National Taiwan University, Taipei, Taiwan, [3]Department of Geological Sciences, University of Oregon, Eugene, OR, USA, [4]Institute of Geology, China Earthquake Administration, Beijing, China

Abstract Characterizing the 700 km wide system of active faults on the Shan Plateau, southeast of the eastern Himalayan syntaxis, is critical to understanding the geodynamics and seismic hazard of the large region that straddles neighboring China, Myanmar, Thailand, Laos, and Vietnam. Here we evaluate the fault styles and slip rates over multi-timescales, reanalyze previously published short-term Global Positioning System (GPS) velocities, and evaluate slip-rate gradients to interpret the regional kinematics and geodynamics that drive the crustal motion. Relative to the Sunda plate, GPS velocities across the Shan Plateau define a broad arcuate tongue-like crustal motion with a progressively northwestward increase in sinistral shear over a distance of ~700 km followed by a decrease over the final ~100 km to the syntaxis. The cumulative GPS slip rate across the entire sinistral-slip fault system on the Shan Plateau is ~12 mm/year. Our observations of the fault geometry, slip rates, and arcuate southwesterly directed tongue-like patterns of GPS velocities across the region suggest that the fault kinematics is characterized by a regional southwestward distributed shear across the Shan Plateau, compared to more block-like rotation and indentation north of the Red River fault. The fault geometry, kinematics, and regional GPS velocities are difficult to reconcile with regional bookshelf faulting between the Red River and Sagaing faults or localized lower crustal channel flows beneath this region. The crustal motion and fault kinematics can be driven by a combination of basal traction of a clockwise, southwestward asthenospheric flow around the eastern Himalayan syntaxis and gravitation or shear-driven indentation from north of the Shan Plateau.

1. Introduction

The region southeast of the eastern Himalayan syntaxis (EHS), including the Shan Plateau, has developed one of the most complex active fault systems within and around the Tibetan Plateau (Shi et al., 2014; Taylor & Yin, 2009). The Shan Plateau between the Red River and Sagaing faults contains two sets of active strike-slip faults (Figure 1). The dominant set consists of the NE-trending, arcuate sinistral-slip faults that occupy an area of 700-by-400 km and straddle neighboring regions of China, Myanmar, Laos, Thailand, and Vietnam. In general, these sinistral-slip faults are longer, wider than the subordinate set of NW- to nearly N-trending dextral-slip faults (Figure 1). The dextral-slip faults dominate the areas adjacent to the Sagaing and Red River faults, suggesting some relationship to these boundary faults.

At least some of these strike-slip faults have a complex kinematic history associated with the tectonic evolution of the India-Asia collision, including a reversal of the sense of slip on the Red River fault sometime between ~17 and ~5 Ma (Lacassin et al., 1997, 1998; Tapponnier et al., 1982, 1986). Constraints on the timing of this tectonic reversal are poor but critical for assessing regional seismic hazard, fault kinematics, and geodynamics, because the timing of the reversal, together with the largest geomorphic/geologic offsets, is commonly used to derive average slip rates (Lacassin et al., 1998; Wang et al., 2014).

The dynamic mechanisms that drive the crustal/lithospheric deformation and associated fault motions on the Shan Plateau are largely debated. Proposed geodynamic mechanisms include crustal shear-driven regional bookshelf faulting and lower crustal or asthenospheric flow and related deformation of overlying crust. The regional bookshelf faulting model (Lacassin et al., 1998; Leloup et al., 1995; Tapponnier et al., 2001)

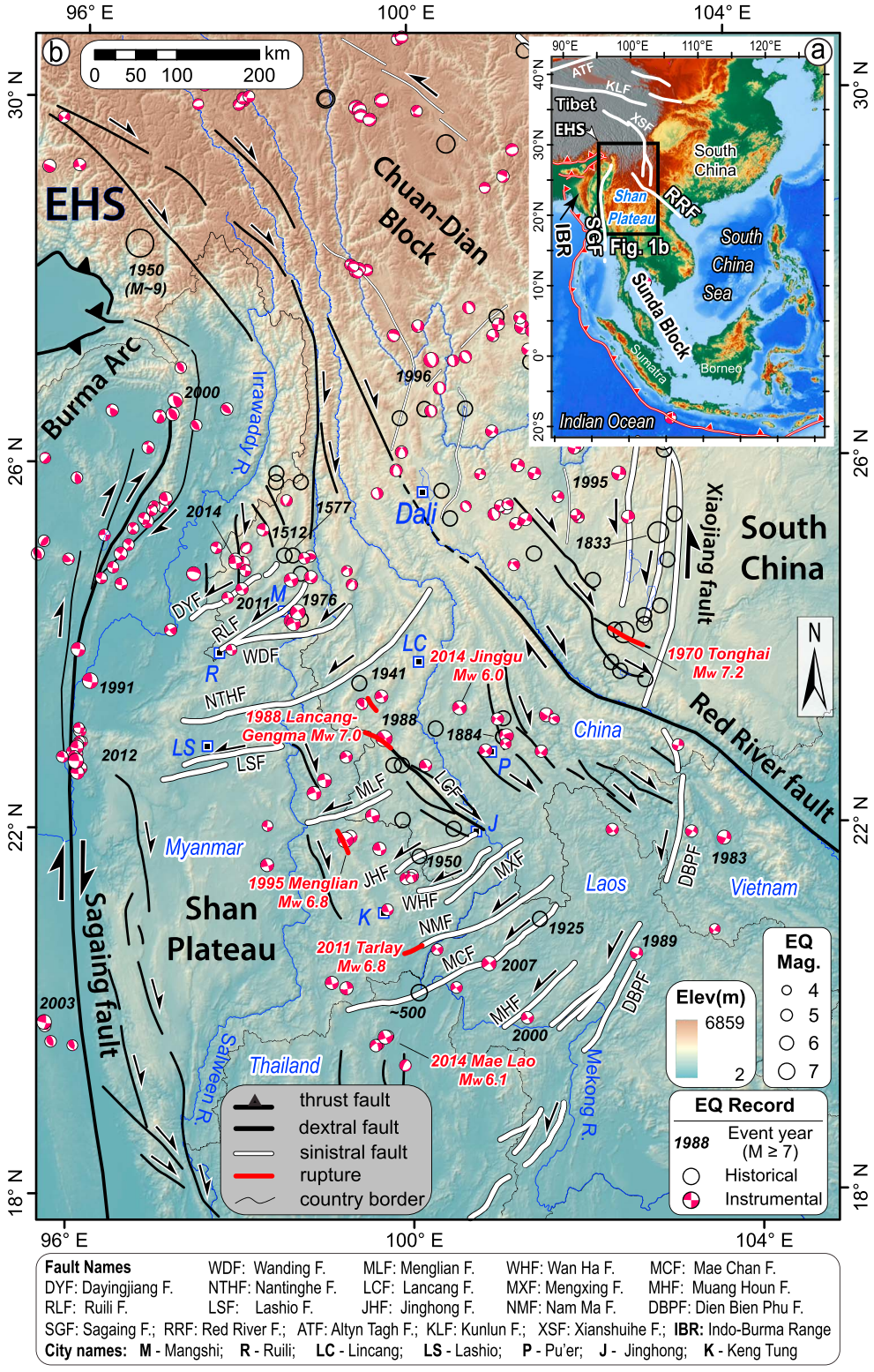

Figure 1. The Shan Plateau, southeast of the eastern Himalayan syntaxis (EHS), has a complex fault system associated with high seismicity (Dziewonski et al., 1981; Ekström et al., 2012; Gu, Lin, Shi, & Li, 1983; Gu, Lin, Shi, & Wu, 1983). (a) The location of the Shan Plateau region within the tectonic context of SE Asia. (b) Active faults and earthquakes on the Shan Plateau. The fault traces are modified from Wang et al. (2014). Surface rupture distribution of earthquakes and their moment magnitudes are derived from (Chen & Wu, 1989; Ji et al., 2017; Pacheco & Sykes, 1992; Tun et al., 2014; Yu et al., 1991; Zhang & Liu, 1978). Note how the sinistral-slip faults curve in arcs around the EHS and how the nodal planes of the earthquakes rotate with them. Dextral-slip faults generally are parallel and close to the Red River and Sagaing faults and are radial to the EHS.

argues that the faults are driven by large-scale simple shear of the block between the dextral-slip Red River and Sagaing faults (Figure 1), perhaps as a consequence of southeastward block extrusion of crustal material (Tapponnier et al., 1982) due to the indenting of the India into Asia. Dynamic flow models interpret the upper-crustal deformation and associated fault development as due to various types of flow around the EHS. These flow models include deep crustal flow induced by crustal thickening (Clark & Royden, 2000; Shen et al., 2005), gravitational spreading flow (Copley, 2008; Copley & McKenzie, 2007), or asthenospheric flow because of the retreat of, and/or corner flow around the Sunda/Burma slab (Li et al., 2008; Sternai et al., 2014; Wang et al., 2013). Basal traction due to deep flow processes can explain the geometry of faults and clockwise rotation of some crustal blocks around the EHS that have been previously observed (e.g., Wang et al., 1998; Wang & Burchfiel, 1997).

To a large degree, discriminating between and quantifying these geodynamic models is difficult because the rates and patterns of fault slip and timing of the initiation of the faults on the Shan Plateau are poorly constrained. Million-year-scale rates determined from offsets of major rivers, ridges, and plutons (Lacassin et al., 1998; Wang et al., 2014) rely on the poorly known age of the slip-reversal event. Millennial slip rates, based largely on thermo-luminescence ages of displaced young alluvial fans and terraces, exist for only the Dayingjiang (Chang et al., 2011), Ruili (Huang et al., 2010), and Wanding (Chang et al., 2012) faults (Figure 1). On decadal timescales, geodetic slip rates have been proposed for the Nantinghe and Lancang faults (Shen et al., 2005; Wang, Wang, et al., 2008). However, these estimates oversimplified the fault geometry and consider neither nearby active faults nor likely postseismic effects of the recent 1988 M ~ 7.6 and M ~ 7.2 Lancang-Gengma earthquakes (Chen & Wu, 1989).

Here we first evaluate and summarize the millennial-to-modern activities of the sinistral-slip faults. We then examine the spatial pattern of the Global Positioning System (GPS) velocity field and constrain the total geodetic strain rate across the entire sinistral-slip fault system by reanalyzing previously compiled GPS data. Following this, we compare the geodetic velocity field relative to the Sunda plate (Kreemer et al., 2014) with the velocity field generated by our reestimated million-year-scale fault activity. Finally, we utilize our key observations of fault geometry, long- and short-term slip rates, and their spatial patterns (i.e., curvature and rate gradients) to evaluate the fault kinematics and existing geodynamic models.

2. Millennial-Scale and Modern Activity of the Sinistral-Slip Faults

Although cumulative offsets up to tens of kilometers along the faults on the Shan Plateau (Lacassin et al., 1998; Wang et al., 2014) suggest that they have been active over millions of years, questions exist whether they remain active (Burchfiel & Chen, 2012), and if so, whether their rates have changed. In this section, we combine evidence from historic and instrumental seismicity, paleoseismic trench studies, and morphotectonic interpretations of small-to-moderate-scale fault offsets (1–1,000 m) to assess the fault activities on different timescales.

2.1. Historic and Instrumental Seismicity

Numerous damaging earthquakes have occurred during the historic and instrumental periods on both the sinistral- and dextral-slip faults throughout the Shan Plateau region (Figure 1), suggesting that many (if not all) of these faults are active today. Examples of recent significant earthquakes on the sinistral-slip faults, from northwest to southeast, include the 2011 M_w 5.5 (Ekström et al., 2012) Yingjiang earthquake on the Dayingjiang fault (Fang et al., 2011; Lei et al., 2012), the 1976 M_w 6.7 and 6.6 earthquake sequence on the Longling-Ruili or nearby sinistral-slip faults (Dziewonski et al., 1981; Gu, Lin, Shi, & Wu, 1983; Guo et al., 2002; Zuo et al., 1996), the 1950 M ~ 7 Daluo earthquake close to the central Jinghong fault near China/Myanmar border (Gu, Lin, Shi, & Li, 1983), the 2011 M_w 6.8 Tarlay earthquake at the western end of the Nam Ma fault (Tun et al., 2014), the 2014 M_w 6.1 Mae Lao earthquake on the Mae Lao fault (~30 km south of the Mae Chan fault) in northern Thailand (Pananont et al., 2017), and two moderate historic earthquakes along the Muang Houn fault zone in northern Laos (Pailoplee et al., 2013) (Figure 1 and Table 1). Moderate earthquakes that have occurred on the dextral-slip faults on the Shan Plateau include the 2014 M_w 5.7 and 5.9 earthquakes north of the Dayingjiang fault (Figure 1) (Ekström et al., 2012; Yang et al., 2016), the 1988 M_w 7.0 Lancang-Gengma earthquake (Chen & Wu, 1989), the 1995 M_w 6.8 Menglian earthquake along a nearly NW-trending dextral-slip fault to the south of the Menglian fault (Ji et al., 2017), and the 2014 M_w

Journal of Geophysical Research: Solid Earth

10.1002/2017JB015206

Table 1
Fault Information and Pleistocene-Holocene Activity of the Sinistral-Slip Faults on the Shan Plateau

Fault name	Code	Fault length (km)	Max. offset[a](km)	Slip rate (mm/year) Over 5 Ma[a]	Over 8 Ma	Over 10 Ma	Over 13 Ma	Evidence for the Pleistocene-Holocene fault activity
Dayingjiang fault	DYF	135	4.1	1.4	0.9	0.7	0.5	Systematic horizontal fault offsets of 20–40 m across streams and alluvial fans; vertical fault offsets in Pleistocene-Holocene sediments (Chang et al., 2011); recent earthquakes along the DYF include the 2011 M_w 5.5 earthquake (Ekström et al., 2012; Fang et al., 2011; Lei et al., 2012) (Figure 1).
Ruili fault east	RLF	100	10.0	2.0	1.3	1.0	0.8	Systematic horizontal fault offsets of 8–70 m across streams and alluvial fans; vertical fault offsets in Pleistocene-Holocene sediments (Huang et al., 2010); earthquakes occurring during the Holocene (He et al., 2014) and modern time (e.g., the 1976 M_w 6.7 and 6.6 earthquake sequence (Dziewonski et al., 1981; Gu, Lin, Shi, & Wu, 1983; Guo et al., 2002; Zuo et al., 1996) (Figure 1).
Wanding fault	WDF	170	10.0	2.0	1.3	1.0	0.8	Systematic horizontal fault offsets of 40–1,100 m across streams and alluvial fans; vertical fault offsets in Late Pleistocene sediments (Chang et al., 2012).
Nantinghe fault	NTHF	380	21	4.2	2.6	2.1	1.6	Systematic horizontal fault offsets of 60–2,000 m across streams and alluvial fans (Shi et al., 2014); Earthquakes occurring during the Pleistocene and Holocene (Shi et al., 2014; Sun et al., 2017). An earthquake also occurred in 1941, immediately south of the NTHF (Figure 1).
Menglian fault	MLF	120	5.5	1.1	0.7	0.6	0.4	Horizontal fault offsets of 90–600 m across streams and fluvial terraces (He et al., 2015); vertical fault offsets and earthquake ruptures observed in Holocene sediments (He et al., 2015).
Jinghong fault	JHF	110	11.0	2.2	1.4	1.1	0.8	Horizontal fault offsets of ~80–610 m across streams and alluvial fans (Figure 2 in this paper); an earthquake with magnitude of ~7 occurred along the JHF on 3 February 1950 (Figure 1).
Wan Ha fault	WHF	140	5.8	1.0	0.6	0.5	0.4	Horizontal fault offsets of ~100–1,000 m across streams and alluvial fans (Figure 2 in this paper).
Meng Xing fault	MXF	180	24.0	4.8	3.0	2.4	1.8	Horizontal fault offsets of ~110–1,300 m across streams and alluvial fans (Figure 2 in this paper).
Nam Ma fault	NMF	215	13.0	2.6	1.6	1.3	1.0	The 2011 M_w 6.8 earthquake occurred along the westernmost NMF in Myanmar (Tun et al., 2014).
Mae Chan fault	MCF	310	4.0	0.8	0.5	0.4	0.3	Horizontal fault offsets of 6–600 m across Streams (Wood, 2001; Weldon et al., 2016); one earthquake occurred during the Holocene (Weldon et al., 2016), possibly around 500 Common Era (Wood, 2001; Penth, 2006; Fenton et al., 2003) and another two moderate earthquakes occurred in 1925 and 2007 (Figure 1)
Muang Houn fault	MHF	158						An M ~ 6.5 earthquake occurred in 1935 (Pailoplee et al., 2013) and another M_w 5.4 earthquake occurred in 2000 (Figure 1) along the MHF in the Laos
Dien Bien Phu fault (Vietnam)	DBPF	150	12.0	2.4	1.5	1.2	0.9	Horizontal fault offsets of 6–150 m of Holocene Age (Zuchiewicz et al., 2004), and 600 m to >1 km of Pleistocene Age (Lai et al., 2012; Zuchiewicz et al., 2004) across streams and fluvial/alluvial terraces; earthquakes occurred during the Holocene (Nualkhao et al., 2016) and modern time along the DBPF (Lai et al., 2012; Figure 1); geodetic rate of sinistral-slip at 1.8 ± 0.3 mm/year (Nguyen et al., 2013)
Total			120.4	24.5	15.3	12.3	9.4	

[a]Data from Wang et al. (2014).

6.0 Jinggu earthquake along a dextral-slip fault to the east of the Lancang fault (Ekström et al., 2012; Xu et al., 2015). In addition, small earthquakes (local magnitudes down to 3) in southwestern Yunnan area, recorded in the China Seismic Network Earthquake Catalog since 1970 (http://www.csndmc.ac.cn/data/dir/china/main) demonstrate widespread small and shallow earthquakes across the entire Shan Plateau fault system. Although only a few of these events have documented surface rupture (the 1988, 1995, and 2011 earthquakes in Figure 1), their fault plane solutions and intensity distributions match well the strikes of geomorphically mapped active faults.

2.2. Millennial Fault Activities Inferred From Paleoseismology

Fault ruptures and associated paleoearthquakes found in trench-exposed and radiocarbon-dated stratigraphy, along/across the fault zones on the Shan Plateau, demonstrate that faults from the entire Shan Plateau region have been active on millennial to centennial timescales. Here we summarize published paleoseismic studies along all sinistral-slip faults in this region (see summary in Table 1). In the northern-central part of the Shan Plateau, He et al. (2014) show that the northeastern section of the Ruili fault had an earthquake 1150 ± 30 years before present (B.P.). Four earthquakes occurred on the central Menglian fault, at ~12,970 years B.P., 4,130 years B.P., between 3,510 and 2,490 years B.P., and between 1,860 and 1,090 years B.P (He et al., 2015). At least five earthquakes occurred along the northeastern Nantinghe fault since the Late Pleistocene, at ≥40,980 years B.P., 40,450–39,170 years B.P., 30,425–7,395 years B.P., 5,485–1,150 years B.P., and 630–515 years B.P. (Sun et al., 2017). In the southeastern part of the Shan Plateau, several studies reveal that the central Mae Chan fault had one earthquake at ~500 Common Era at a site 20 km east of Mae Chan (Penth, 2006) and at least two earthquakes in the last 9,000 years (Weldon et al., 2016). Along the Xaignabouli fault zone, a branch of the central Dien Bien Phu faults in western Laos, three earthquakes occurred at ~3,000, 2,000, and 1,000 years ago (Nualkhao et al., 2016), dated by optically stimulated luminescence (Aitken, 1998) of fault-rupture related sediments.

2.3. Millennial Fault Activities Inferred From Moderate Fault Offsets

Morphotectonic mapping along all sinistral-slip faults on the Shan Plateau also show clear signs of millennial-scale fault activities. For commonly observed average slip rates of a few mm/year, strike-slip faults will accrue offsets from meters to thousands of meters, over 10^3–10^6 years. Therefore, a range of offsets across geomorphic markers (e.g., streams, ridges, terraces, and alluvial fans) of different ages are good indicators that they were active over thousands to millions of years. Previous studies have already shown a range of offsets (several to thousands of meters) accumulated along the faults near the northwestern (Chang et al., 2011, 2012; He et al., 2014; Huang et al., 2010; Shi, 2014) and southeastern (Lai et al., 2012; Nualkhao et al., 2016; Weldon et al., 2016; Wood, 2001; Zuchiewicz et al., 2004) parts of the Shan Plateau.

For several faults (i.e., the Jinghong, Wan Ha, and Meng Xing faults; Figure 2) in the central Shan Plateau that lack existing studies, we have mapped and present their small-to-moderate offsets that reflect the faults' millennial activities using 30 and 5 m resolution digital elevation models produced from the Shutter Radar Topography Mission data and from optical imagery of the Advanced Land Observation Satellite, respectively. We delineate active fault traces by recognition of linear, continuous geomorphic features with narrow valleys, linear ridges, and systematic offsets of geomorphic markers (streams, ridges, terraces, and alluvial fans) along the traces, and systematic topographic changes in slope across the linear traces. Our measurements based on the Shutter Radar Topography Mission and Advanced Land Observation Satellite digital elevation models demonstrate that these faults in the central section of the Shan Plateau produce sharp and accumulated offsets across streams and river terraces, ranging between ~80 and ~1,300 m (Figure 2 and Table 1). The resolution of our imagery precludes systematically mapping meter-scale offsets.

Collectively, our summary of previous paleoseismological and geomorphic studies on many of the sinistral-slip faults, and our new work on several additional faults on the central part of the Shan Plateau, suggests that all these faults were active on millennial timescales. Together with previous inference of their activities on million-year timescale (Lacassin et al., 1998; Wang et al., 2014) and our review of historic and instrumental seismicity of these Shan Plateau faults, we therefore suggest that all sinistral-slip faults included in Figure 1 on the Shan Plateau have been active since their initiation of sinistral slip, which provides an important constraint on the fault kinematics and regional geodynamics.

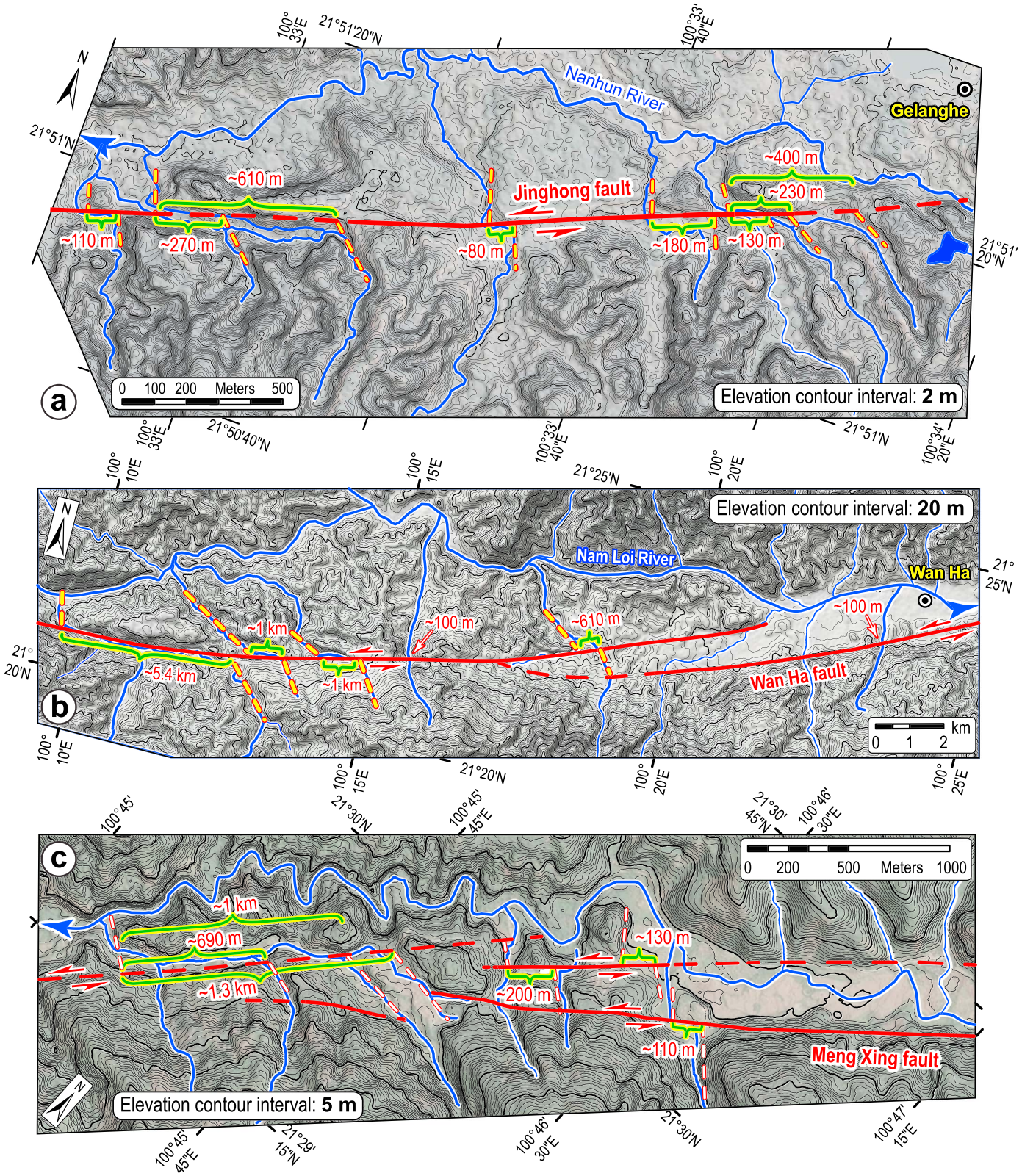

Figure 2. The range of small to large offsets along the sinistral-slip faults on the central Shan Plateau indicates continuous activity during the Quaternary. (a) Fault offsets of streams and alluvial fans near Gelanghe town along the northeastern section of the Jinghong fault. (b) Stream offsets near Wan Ha village, Myanmar, along the southwestern section of the Wan Ha fault. (c) Stream offsets at a site ~5 km northeast of Bok Hsopnam village, Myanmar, along the northeastern section of the Meng Xing fault. The blue lines in all three maps show the tributary network of the Mekong River.

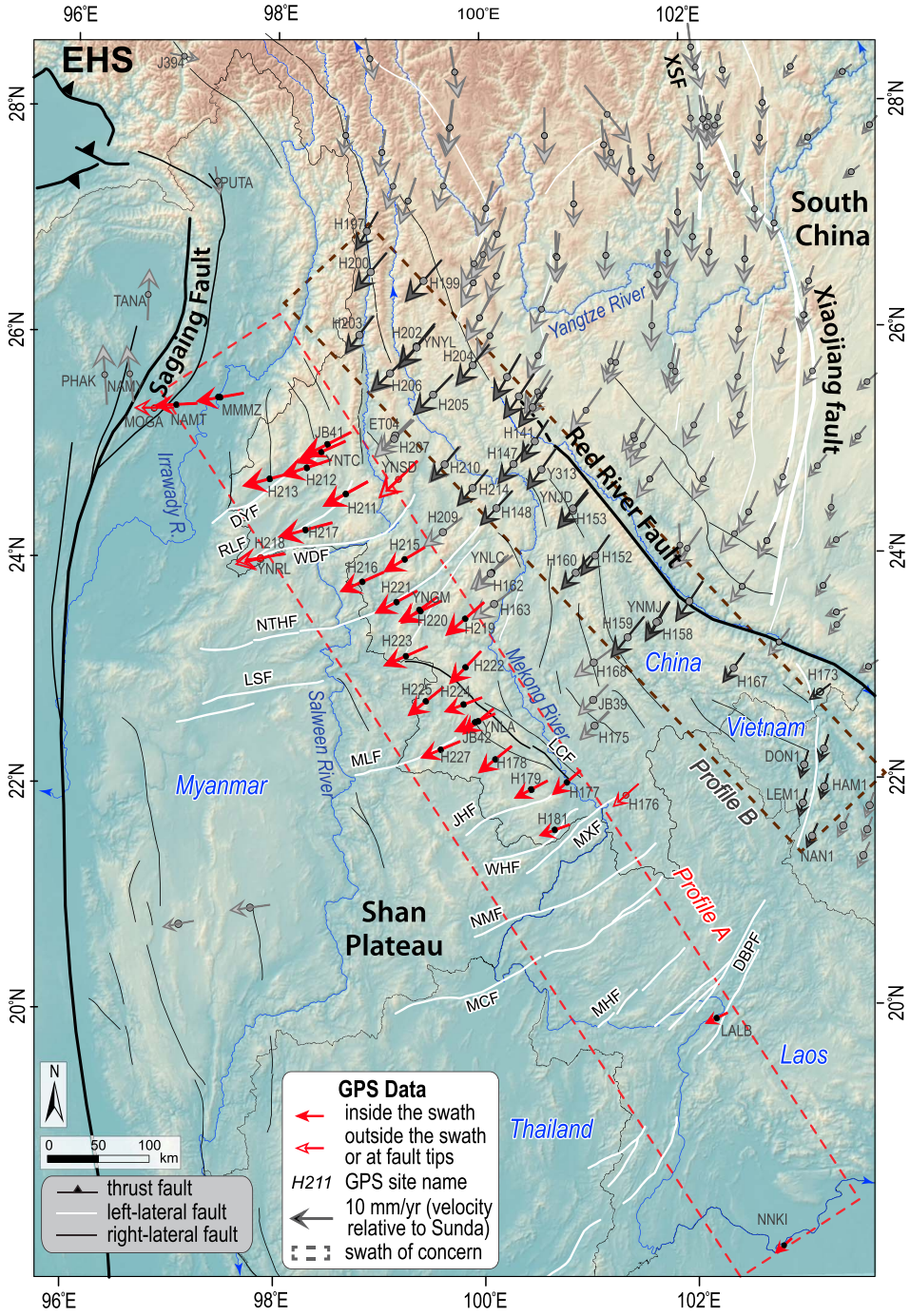

Figure 3. GPS velocity vectors relative to the Sunda reference frame (Kreemer et al., 2014) with fault traces in this region. Fault names in Figure 1. Note that the velocity vectors rotate around the EHS and are parallel to the sinistral-slip faults. The dashed box-bounded red and black arrows show GPS data plotted in velocity profiles on Figure 4.

3. GPS Velocity Field

3.1. GPS Data Analysis

To best constrain the current velocity field, we chose 47 campaign-mode and 10 continuous GPS stations within two swaths, one across the central sinistral-slip fault system and the other across a domain of dextral faults (Figure 3). The GPS data in southwestern China, northern Laos, and Vietnam come from three studies (Liang et al., 2013; Nguyen et al., 2013; Shen et al., 2005). Additional GPS data are from northern Myanmar

Maurin et al. (2010) and northern Thailand (Simons et al., 2007). All velocity vectors have been reprojected by Kreemer et al. (2014) from ITRF2008 to the Sunda reference frame. We chose to use the Sunda reference frame, as the Shan Plateau itself is within the Sunda plate. The GPS vectors relative to the Sunda block are similar in orientation and magnitude to those relative to the South China block (Shen et al., 2005), which has very limited motion relative to the Sunda plate.

Most campaign-mode GPS stations have at least five observational campaigns over >10 years and the continuous stations in China and Laos span 2010–2013 (Table 1 in Liang et al., 2013). The campaign stations in northern Myanmar and northern Vietnam were measured during 2005–2008 (Maurin et al., 2010) and 2002–2012 (Nguyen et al., 2013), respectively. To compare the decadal-scale to million-year-scale slip rates on the sinistral faults, we projected the horizontal GPS velocity vectors onto the average strike (240°N) of the sinistral-slip fault system along a profile perpendicular to the faults.

3.2. Spatial Pattern of GPS Velocities and Total Geodetic Slip Rate Across the Shan Plateau

Two important spatial patterns can be observed in the regional-scale GPS velocities. First, the GPS vectors show a clockwise rotation around the EHS (Figure 3), as has been noted in previous studies (e.g., Shen et al., 2005). This rotation smoothly continues across the Red River fault, without a measurable change in their vector directions or magnitudes, suggesting little motion along the Red River fault. Second, most of the GPS velocities north of the Red River fault show only small variations in both E-W and N-S directions, suggesting block-like motion. In contrast, the GPS velocities southwest of the Red River fault show large systematic variations, suggesting distributed motion.

GPS velocity profiles show a clear tongue-like pattern in the GPS rates across the Shan Plateau (Figure 4). Along Profile A across the sinistral-slip faults, the velocities relative to the Sunda plate are relatively low and flat for a distance of ~200 km (between stations LALB and NNKI) away from the Dien Bien Phu fault zone, the southeastern margin of the sinistral-slip system. The velocities then progressively increase northwestward from near the Dien Bien Phu fault, followed by a velocity decrease in the last 100 km of the profile (Figure 4). Although the GPS velocities at the northernmost sites MOGA and NAMT may be affected by the elastic deformation associated with the Sagaing faults, our first-order calculation based on an elastic dislocation model (Savage & Burford, 1973) suggests that strain accumulation across the Sagaing faults has a minor effect (<1 mm/year; Figure S1) at MOGA and NAMT sites, compared to the magnitude of the apparent velocity reversal (>5 mm/year) found in Profile A.

GPS velocities along Profile B, which crosses several sinistral-slip and the main group of dextral-slip faults and ends about 200 km from the Sagaing faults, show a similar velocity variation to Profile A. Therefore, we infer that the gradual increase followed by a reversal of velocity gradient is an important aspect of the kinematics of the Shan Plateau region and provides an important clue to geodynamics. The fact that Profile B largely crosses a domain of dextral-slip faults but still shows the same pattern in rate, rate gradient and curvature as Profile A across the sinistral-slip faults suggests both types of faults accommodate the same strain.

From both GPS profiles, we constrain the cumulative sinistral-slip rate across the entire sinistral-slip fault system, from the Dien Bien Phu to the Dayingjiang faults, as ~12 mm/year (Figure 4). This rate, when divided by 14, the total number of major sinistral faults across the system, yields an average slip rate of ~1 mm/year for individual faults within the Shan Plateau region. Because average slip rate is within one-sigma uncertainties of individual campaign GPS velocities (as large as 1.5 mm/year), it is impossible to determine individual fault slip rates from the current GPS data alone. Nonetheless, the cumulative slip rate and the relative gradients are robust across the Shan Plateau region.

4. Long-Term Fault Slip Rates

Long-term fault offsets across each major sinistral-slip fault on the Shan Plateau have been estimated, and the total across the entire system is 110–130 km (Lacassin et al., 1998; Wang et al., 2014). To calculate the slip rates, the sinistral-slip faults are assumed to initiate concurrently with the slip reversal (from sinistral to dextral) of the Red River fault (Leloup et al., 1993). However, estimates of the timing of the slip reversal remain uncertain.

Leloup et al. (1993) proposed that the slip reversal occurred at ~5 Ma. This age is estimated from the onset time of the normal faulting in the Dali area (Figure 1) that was interpreted to be kinematically associated

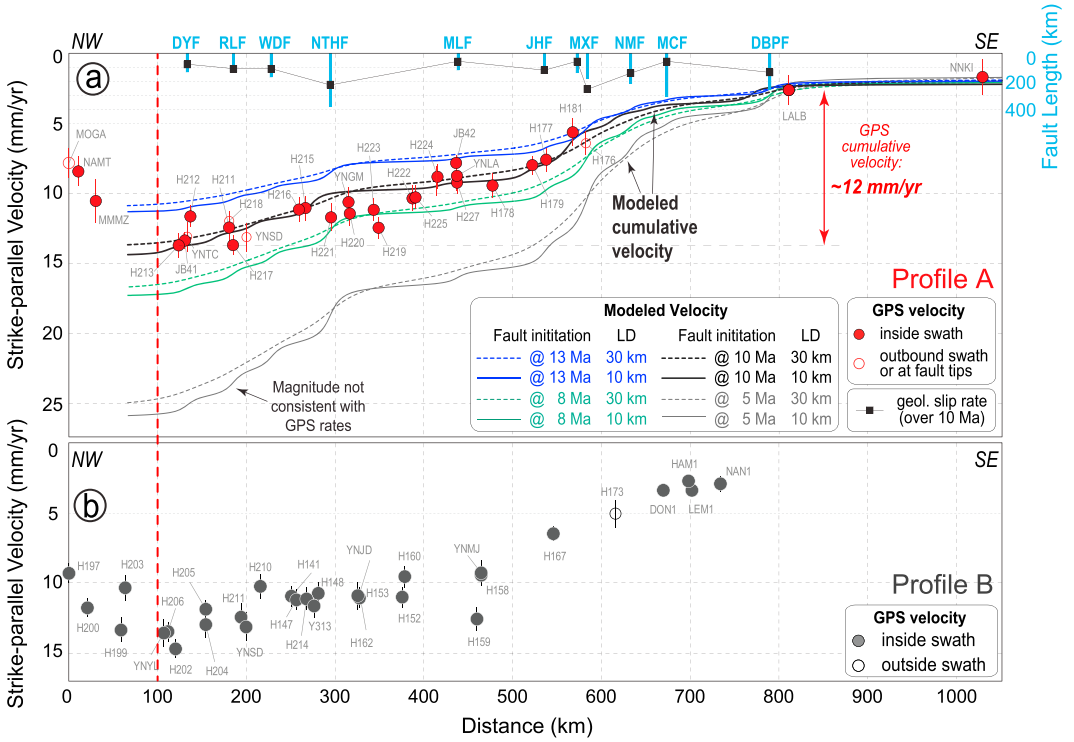

Figure 4. GPS velocity profiles across the Shan Plateau. (a and b) The spatial pattern of GPS velocities projected onto the average strike of the sinistral fault system, along Profiles A and B, respectively. Note that GPS velocities progressively increase toward the EHS but then decrease slightly at the northwestern end of each profile, and that while the Profile B domain is dominated by dextral-slip faults, it shows the same velocity pattern as Profile A. Shear directions are consistently parallel to the sinistral-slip faults and orthogonal to the dextral-slip faults. Also shown in (b) is the modeled surface velocity field, which is consistent with the GPS data and calculated based on (1) a simple elastic dislocation model (Savage & Burford, 1973), assuming a range of locking depths of 10–30 km and, and (2) geological slip rates (marked in black squares) obtained from observed maximum kilometer-scale channel/ridge offsets (Wang et al., 2014) divided by proposed onset time of faulting at ~5 (Leloup et al., 1993), 8, 10, or 13 Ma (Li et al., 2013; Wang et al., 2001). Fault names in Figure 1.

with the start of the dextral slip of the Red River fault. In this case, division of the total estimated sinistral offsets of 110–130 km (Wang et al., 2014) by this age yields a million-year-averaged cumulative slip rate of ~24 ± 2 mm/year (Figure 4a and Table 1), across the entire sinistral-slip fault system; this rate is double the cumulative geodetic rate (Figure 4a).

More recent studies suggest an earlier onset of the normal faulting in the region, between 8 and 13 Ma. Lines of evidence for the earlier onset include basal ages (~8 Ma) of extensional subbasins related to strike-slip faulting in the northern Dali basin (Li et al., 2013) (Figure 1), and the onset of rapid bedrock cooling at ~13 Ma inferred to be induced by normal faulting and exhumation (Cao et al., 2011) near the northwestern Red River fault zone (Figure 1). Following the same assumptions of previous studies (Lacassin et al., 1998; Leloup et al., 1993; Wang et al., 2014), these observations suggest that the current sinistral faults on the Shan Plateau started concurrently with the normal faulting in Dali area at 8 or 13 Ma. Dividing these ages from the total estimated sinistral offsets (110–130 km) (Wang et al., 2014) provides a long-term cumulative slip rate across the entire fault system of 8–16 mm/year (Figure 4a and Table 1). It is important to note that the long-term rate is indistinguishable from the rate derived from the GPS geodetic rates, if the faults initiated at ~10 Ma (Figure 4a).

5. Comparison of Gradient Patterns Between Geological and Geodetic Velocity Field

We can use individual estimates of fault slip rate to generate cumulative geologic velocity field across the fault system, using an elastic dislocation model (Savage & Burford, 1973) that assumes a locking depth of either 10 or 30 km (Figure 4a), to compare to the geodetic velocity field. Our results show that the

modeled velocity fields for the different locking depths are similar within the uncertainties (up to 1.5 mm/year) of the GPS measurements. The differences in the velocity fields, under assumptions of different ages for the fault initiation (e.g., at 5, 8, 10, and 13 Ma), exist mainly in the magnitude of the modeled velocity field (Figure 4a). The best fit appears for fault initiation at ~10 Ma. The velocity field with fault initiation at ~5 Ma doubles the geodetic rate. Subtle variations in slope can be observed between the modeled and geodetic velocity profiles, suggesting variations in fault slip rates. Discrepancies in the region south of the Nantinghe fault might be associated with the postseismic deformation following the M_w 7.0 Lancang-Gengma earthquake of 1988 (Figure 1) (Chen & Wu, 1989).

Importantly, no matter when the faults initiated, and whether rates on individual faults vary on million-year timescales, the spatial pattern of the derived velocities from multimillion slip rates (i.e., progressively northwestward increase across the entire set of sinistral-slip faults) is consistent with that observed in the GPS data (Figure 4a). Such consistency suggests that the same geodynamic processes have been driving the fault kinematics since the initiation of the sinistral-slip faulting.

6. Discussion

All regional geodynamic models must explain the arcuate geometry of sinistral-slip faults, their spacing, and spatial distribution in slip sense, the fact that the dextral-slip faults accommodate the same shear as the sinistral-slip faults, and the curved tongue-like deformation field defined by the active faults, GPS velocities, and geological slip gradients (Figure 4) observed in this study. We now use these observations to discuss kinematics and geodynamic models for this region.

6.1. Fault Kinematics

Based on our and Wu et al. (2015)'s observations, the Shan Plateau and adjacent regions may be simplified into six domains characterized by groups of similar fault geometry and structural styles. From north to south, these zones (Figure 5a) include (1) the southern part of the Chuan-Dian (Sichuan-Yunnan) block (Xu et al., 2003) that contains mainly the S- and SE-trending sinistral-slip faults (Zone A); (2) the domain that contains the arcuate north-south-trending dextral-slip faults, immediately to the southeast of the EHS and bounded by the Sagaing fault, Dayingjiang fault, and a boundary that separates the dextral- and sinistral-slip faults (the thick black dashed line in Figure 5a, referred as "D-to-S boundary") (Zone B); (3) the arcuate sinistral-slip faults from the Nantinghe to the Dayingjiang faults (Zone C); (4) the NE-trending sinistral-slip faults between the Nantinghe and Dien Bien Phu faults (Zone D); (5) the NNW-trending dextral-slip faults between Zone C and the Sagaing fault (Zone E); and (6) the SE-trending dextral-slip faults bounded by the Red River, Lancang, Nantinghe, and Dien Bien Phu faults (Zone F).

Based on fault styles of these domains, the present-day fault network of the Shan Plateau may be simplified as subfaulted blocks of different sizes (Figure 5b), developed from preexisting structures (Lacassin et al., 1997, 1998). It is important to notice that the fault network shows a radial pattern around the EHS (Figures 5b and 6a). That is, 11 out of 14 of major sinistral-slip faults on the Shan Plateau follow concentric curves around one single pole in the EHS (Figure 6a); and the dextral-slip faults trend approximately perpendicularly to those concentric curves. Both the sinistral- and dextral-slip faults accommodate the same strain as demonstrated by the GPS velocity profiles (Figures 3 and 4).

These faulted domains show different kinematics. Zone A of the Chuan-Dian block demonstrates a block-like large-scale rotation and indentation into the Red River fault (Figure 5c), as reflected by small variations of GPS velocities within the block (Figure 3) and argued in previous studies (Su et al., 2011; Wang et al., 1998). Zone B is mainly characterized by a large clockwise rotation around a pole anchored near the EHS (Molnar & Lyon-Caen, 1989). Zones C to F are consistent with a differential shear (Figure 5d) from the relative large (~12 mm/year) differential slip between the Dayingjiang and Dien Bien Phu faults (Figure 1), as demonstrated by the GPS velocity patterns (Figure 4). Importantly, regional tongue-like curved shear exerting on preexisting structures (Figure 5d) can drive both the sinistral- and dextral-slip faults observed on the Shan Plateau. The shear-driven rotations of the fault-bounded microblocks can also explain the nearly E-W extension at the terminations of the sinistral-slip faults and on the sides of the N- to NW-trending dextral-slip faults (Wang & Burchfiel, 1997; Wang, Wan, et al., 2008).

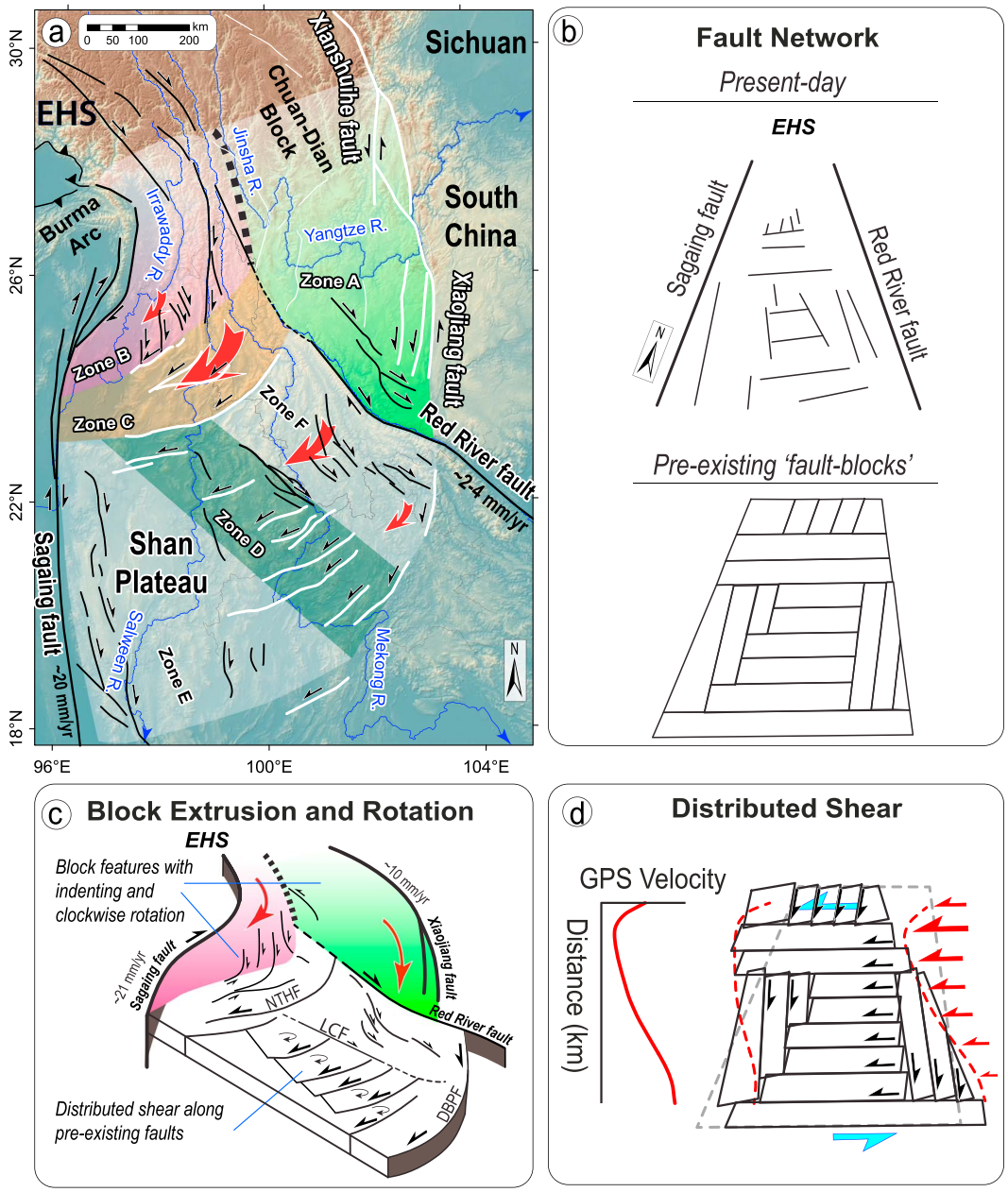

Figure 5. The fault domains and kinematics around the Shan Plateau. (a) Six domains with different fault styles. The thick dashed black line here and also in panel (c) shows the "D-to-S boundary" discussed in the text. (b) Simplified present-day radial pattern of the fault network and preexisting fault structures in the region. (c and d) The domains characterized by block-like rotation and by regional distributed shear, respectively. Note how both the sinistral- and dextral-slip faults can be explained by the distributed shear relating to the curved tongue-like velocity pattern.

6.2. Implications for Regional Geodynamics

The geodynamic mechanisms that drive the crustal motion and associated fault movement around the Shan Plateau region are debated. The controversy is mainly whether the forces are from the shallow crust or deeper in the lithosphere or below. Proposed shallow forces include the horizontal shearing force sourced from the indenting of the India into Eurasia (e.g., Tapponnier et al., 1982) and the gravitational potential energy-induced spreading (e.g., Copley, 2008; England & Molnar, 1997; Molnar & Lyon-Caen, 1988). Deep forces may come from basal traction by flows in the deep crust (Clark et al., 2005; Clark & Royden, 2000; Royden et al., 1997) or asthenosphere (Li et al., 2008; Sternai et al., 2014; Wang et al., 2013). Here we

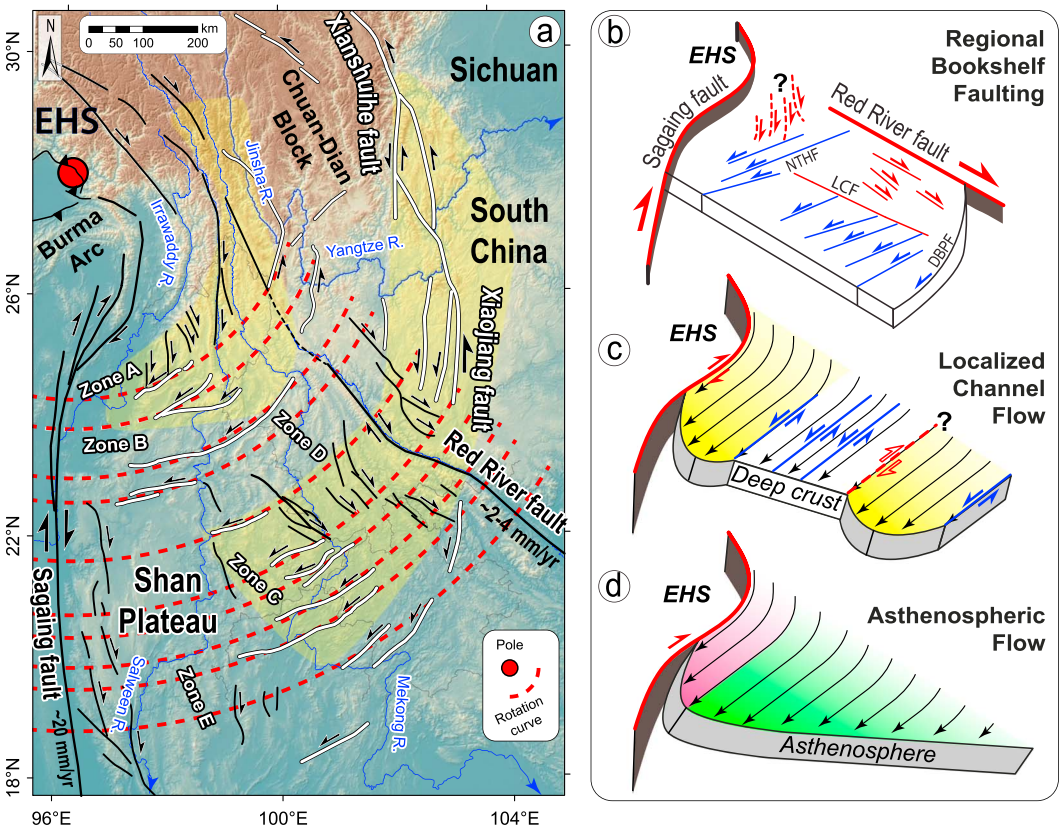

Figure 6. The curved faults around the EHS and proposed geodynamic models for the complex fault systems on the Shan Plateau. (a) Map showing all arcuate sinistral-slip faults except the Wanding and Dien Bien Phu faults follows cocentric curves (red dashed lines) around a pole near the EHS. Note also that the dextral-slip faults are nearly orthogonal to the arcuate concentric curves. The two yellow-shaded areas show the approximate locations of two low-velocity zones that have been interpreted as crustal channel flows (Bao et al., 2015), also refer to panel (c). (b) Regional bookshelf faulting between the Red River and Sagaing faults. (c) The localized deep crustal channel flow model. Note that such a model will develop a dextral-slip fault in parallel with the NE-tending sinstral-slip faults, which contradicts observations of the consistent fault slip sense in this region. (d) The tongue-like asthenospheric flow model. The black arrows show the change in velocities within the flow zone. The pink and green shaded areas show where the flow may drive the crustal motion in corresponding areas in Figure 5c.

attempt to evaluate these mechanisms based on our key observations on the fault geometry, kinematics, and GPS velocities.

6.2.1. Regional Bookshelf Faulting Between the Sagaing and Red River Faults

The first model we evaluate is regional bookshelf faulting (Figure 6b) due to horizontal dextral shear generated by dextral-slip on the Red River and Sagaing faults that bound the northern corner of the Sunda plate (Figure 1) (Lacassin et al., 1997; Leloup et al., 1995; Tapponnier et al., 2001). This model can explain the sense of shear of the sinistral faults and the boundary dextral faults but cannot explain several of our observations. First, this model may generate a curved northwestward regional velocity pattern, but this contradicts to our observation of the asymmetric tongue-like GPS velocity pattern toward to the southwest, which also requires a switch in slip sense from dextral- to sinistral-slip northwest of the Dayingjiang fault. Second, the distinct arcuate shape of the sinistral-slip faults and the curved GPS velocity field across the Red River fault (Figure 3) are difficult to reconcile with regional bookshelf faulting. Finally, this model requires a rapid slip along the Red River fault. Although the Red River fault was a large crustal-scale plate-boundary fault in the geologic past, it has a very low dextral slip rate along its central section over decadal (1–2 mm/year) (Shen et al., 2005; Wang, Wang, et al., 2008) and millennial and million-year (1–5 mm/year) (Replumaz et al., 2001; Schoenbohm et al., 2006; Weldon et al., 1994) timescales. This observation

suggests that this fault cannot play a significant role in providing the needed horizontal simple shear. Thus, the regional bookshelf faulting model is difficult to explain the crustal motion in the Shan Plateau region.

6.2.2. Crustal Shearing Between the Northern Sagaing and Xiaojiang Faults

A variation of the regional bookshelf faulting model could be driven by crustal shearing between northern Sagaing fault and the Xiaojiang fault (Figure 5c). The curved, tongue-like pattern of GPS velocities across northern Sagaing-Xiaojiang fault observed previously (Copley, 2008) may generate southwestward differential shear across the Shan Plateau and hence fault kinematics consistent with our observations (Figure 5d). In this case, indention of the Chuan-Dian block into the central Red River fault can also explain its southwestward deflection, as argued in previous studies (Schoenbohm et al., 2006; Wang et al., 1998).

Such shearing forces may partly relate to the far-field indenting of India into Eurasia (e.g., Tapponnier et al., 1982), the gravitational spreading (e.g., Copley, 2008; England & Molnar, 1997; Molnar & Lyon-Caen, 1988) because of the crustal thickening and uplift of the Tibetan Plateau, and the trench rollback along many of the subduction zones in Southeast Asia (e.g., Hall & Morley, 2004; Royden et al., 2008). To what degree each of these processes contributes to the crustal deformation in the study region requires future acquisition of more geological data and numerical modeling to test.

6.2.3. Localized Crustal Channel Flow

Widespread deep crustal flow has been proposed to explain the $>$1,000 km long southeastward topographic gradient (Figure 1a) from the flat plateau surface (~4,500 m in elevation) northeast of the EHS to the coast of the southwest part of the South China Sea (Clark et al., 2005; Clark & Royden, 2000). However, recent studies show that crustal flow may be localized (Yao et al., 2010), rather than widespread, along two parallel channels at depth of ~21 km beneath southeast of the EHS region (Bao et al., 2015) (Figures 6a and 6c). If localized crustal channel flow exists beneath this region, we would expect to see dextral-slip faults on one side, and sinistral-slip faults on the other side of a flow channel. Thus, some NE-trending dextral-slip faults (dashed line in Figure 6c) would develop in parallel with the NE-trending sinistral-slip faults in central Shan Plateau. This contradicts our observation that the NE-trending faults starting from the Dayingjiang fault to the southeast (Figure 1) are all sinistral.

One may argue that a two-channel crustal flow model may also explain the sinistral-slip fault kinematics, if the faults in the central part of the Shan Plateau are inactive and simply entrained within the channel of flowing crust. However, our summary of the fault activities of the sinistral-slip faults near the margin (Table 1) and new observations of such activities in the central part of the Shan Plateau (Figure 2) suggest that all the major faults are active since their initiation of sinistral-slip faulting. The activities of these faults mean that they cannot be zero-slip-rate free boundaries, against the entrainment of the central Shan Plateau within a flow zone. Therefore, our observations of the southwestward tongue-like crustal motion and fault slip behaviors on the Shan Plateau cannot be reconciled with a localized channel flow model. However, our observations cannot be used to rule out the existence of crustal flow beneath this region; if localized lower crustal flow does exist, other processes dominate the fault kinematics on the Shan Plateau.

6.2.4. Asthenospheric Flow Around the EHS

The model of asthenospheric flow around the EHS has previously been proposed to explain the dynamics in this region (Li et al., 2008; Wang et al., 2013). This asthenospheric flow is likely associated with the retreat of the Sunda subduction zone or by corner flow around the Sunda slab (Li et al., 2008; Wang et al., 2013). The exact origin of the asthenospheric flow, whether it results from local mantle dynamics (e.g., collision-subduction processes, Sternai et al. (2014) or larger-scale mantle convection (e.g., Becker & Faccenna, 2011), is beyond the scope of this study.

Previous observations and interpretations that support this flow model include the following: (1) the crustal thickness of the Shan Plateau region is less than 40 km (Bao et al., 2015), and the lithosphere is around 80 km or less (Pasyanos et al., 2014), which may facilitate coherent lithospheric deformation. (2) Southeastern Tibetan crust is thought to be coupled to the mantle lithosphere, and thus, movement of the entire crust is likely the same as the uppermost mantle; this inference is supported by the mechanical coupling across the upper and lower crust (Copley et al., 2011) and by the similarity of the surface deformation field and seismic anisotropy, which is mainly in the asthenosphere (below 80 km depth), inferred from shear wave splitting

observations (Huang et al., 2015; Wang et al., 2013). (3) Recent 3-D thermo-mechanical numerical models involving processes of continental collision, oceanic subduction, and slab retreat support the role of asthenospheric flow in driving the surface strain, subhorizontal and upward vertical motion around EHS region (Sternai et al., 2014; Sternai et al., 2016). (4) Recent analog models also suggest that the shear traction of the tongue-flow acting at the base of flow zones (e.g., Yin & Taylor, 2011) may drive development of non-Andersonian conjugate dextral- and sinistral-slip faults, observed on the Shan Plateau and in the Chuan-Dian block (Figures 1 and 5a) (Su et al., 2011). (5) A portion of the Mid-Miocene and Quaternary igneous rocks in southwest Yunnan and Myanmar may source from the asthenosphere (e.g., Lee et al., 2016). These findings suggest that the rigidity of the upper crust does not significantly filter the forcing from lower, more ductile layers.

The asthenospheric flow model can explain many aspects of our observations. First, the tongue-like pattern of subsurface flow velocities would produce a gradual increase in horizontal velocities toward the center of the flow zone (Figure 6d). Basal traction from the asthenospheric flow would drive the observed tongue-shaped crustal motion and surface velocity field across both sinistral- and dextral-slip faults on the Shan Plateau (Figure 4). Second, the curved velocity field may cause the southwestward differential shear in the region and consequent faulting along preexisting structures (Figure 5d), and thus can explain the arcuate fault lines and GPS velocities relative to the Sunda plate (Figure 3) that follow concentric curves around a pole near the EHS (Figure 6a). Third, the model is consistent with our observation of comparable magnitudes (~10 mm/year) and style of geodetic deformation across the Red River fault that suggest the same geodynamic process across this fault and its little role in the current deformation. This observation suggests a nearly complete transfer of surface strain from the deformation between the EHS and Xiaojiang fault system, north of the Red River fault, to the broad region characterized by the diffuse deformation among quasi-parallel sinistral faults on the Shan Plateau region. Fourth, the southwestward deflection of the central Red River fault, and the westward deflection of the central Sagaing fault and the Indo-Burma Range (Figure 1), is also consistent with the proposed flow.

It is important to note that, deep forces such as basal traction of asthenospheric flow and from the shallow crustal-shearing induced by indentation of the India into Eurasia plates, the gravitational spreading and far-field trench rollback are not mutually exclusive. The contribution of these different geodynamic processes to crustal motion largely depends on the relative movement of the asthenosphere and the crust, and thus the relative magnitude of various driving forces, as well as the crustal heterogeneities. Therefore, the dominant control of different mechanisms for driving the crustal motion across the Shan Plateau region may vary in time and space. In fact, previous studies show that the fault kinematics in eastern Tibet may relate to a change in the predominant geodynamics of this region during the Middle to Late Miocene (Wang et al., 2012), when the faults around the Shan Plateau region experienced a switch in slip sense. Such a change possibly relates to the fast buckling and deformation of the Indian Ocean lithosphere during this time period (e.g., Molnar et al., 1993). Future data and models are necessary to test and quantify the spatio-temporal changes in roles of different forces in driving crustal motion around the EHS region.

7. Conclusions

We use the kinematics, GPS velocity field, and slip rate gradients of the fault systems on the Shan Plateau over multiple timescales to interpret the kinematics and geodynamics of this region. From our new analysis of previously published GPS data, we observe a curved, southwestward, tongue-like crustal motion that shows a progressively northwestward increase in GPS velocities for an ~700 km long distance then a decrease over the final ~100 km to the syntaxis. We constrain the total geodetic slip rates across the sinistral fault system to ~12 mm/year and an average slip rate of ~1 mm/year for individual faults. The total geodetic slip rate is the same as the cumulative geologic rate averaged over ~10 Ma. Based on the deformation field defined by the active faults, the tongue-like pattern of GPS velocities, and geological slip gradients, the fault kinematics is characterized by a regional southwestward differential shear, compared to more block-like rotation and indentation north of the Red River fault. Our observations of the fault slip and GPS velocities are difficult to reconcile with previously proposed regional bookshelf faulting between the Sagaing and Red River faults and localized deep crustal flow beneath the region. The regional geodynamics appears to be driven by crustal shearing that relates to indenting of the India into Eurasia plates and gravitational spreading to the north and by deep traction due to southwestward directed, clockwise, asthenospheric flow around EHS.

Acknowledgments
This research is supported by Earth Observatory of Singapore (EOS), Nanyang Technological University, through its funding from National Research Foundation Singapore and the Singapore Ministry of Education under the Research Centers of Excellence initiative. The EOS contribution number for this paper is 125. L. Z. J. is supported by National Science Foundation of China project (41761144065). We thank Elise Weldon, Kyle Bradley, Emma Hill, Eric Lindsey, and Wayne Thatcher for beneficial discussions during the preparation of this paper. Comments from Robin Laccasin and several anonymous reviewers helped improve earlier versions of this paper. We also thank the Editor, Paul Tregoning, and the associate editor for handling this paper. Supporting data can be accessed in the supporting information files and related references cited in the text.

References

Aitken, M. J. (1998). *An introduction to optical dating: The dating of Quaternary sediments by the use of photon-stimulated luminescence*. Oxford, New York, Tokyo: Oxford University Press.

Bao, X., Sun, X., Xu, M., Eaton, D. W., Song, X., Wang, L., et al. (2015). Two crustal low-velocity channels beneath SE Tibet revealed by joint inversion of Rayleigh wave dispersion and receiver functions. *Earth and Planetary Science Letters*, *415*, 16–24. https://doi.org/10.1016/j.epsl.2015.01.020

Becker, T. W., & Faccenna, C. (2011). Mantle conveyor beneath the Tethyan collisional belt. *Earth and Planetary Science Letters*, *310*(3–4), 453–461. https://doi.org/10.1016/j.epsl.2011.08.021

Burchfiel, B. C., & Chen, Z. (2012). *Tectonics of the southeastern Tibetan Plateau and its adjacent foreland* (Vol. 210). Boulder, CO: Geological Society of America.

Cao, S., Neubauer, F., Liu, J., Genser, J., & Leiss, B. (2011). Exhumation of the Diancang Shan metamorphic complex along the Ailao Shan-Red River belt, southwestern Yunnan, China: Evidence from 40Ar/39Ar thermochronology. *Journal of Asian Earth Sciences*, *42*(3), 525–550. https://doi.org/10.1016/j.jseaes.2011.04.017

Chang, Z.-F., An, X., & Zhang, Y. (2012). Study on Late-Quaternary activity and displacement of drainage systems along the Wanding fault (in Chinese with English abstract). *Seismology and Geology*, *34*(2), 228–239.

Chang, Z.-F., Chen, G., & Yu, J.-Q. (2011). Geological evidence of activity along the Dayingjiang Fault since late Pleistocene (in Chinese with English abstract). *Seismology and Geology*, *33*(4), 877–888.

Chen, Y., & Wu, F. T. (1989). Lancang-Gengma earthquake: A preliminary report on the November 6, 1988, event and its aftershocks. *Eos, Transactions American Geophysical Union*, *70*(49), 1527–1540. https://doi.org/10.1029/89EO00376

Clark, M. K., Bush, J. W., & Royden, L. H. (2005). Dynamic topography produced by lower crustal flow against rheological strength heterogeneities bordering the Tibetan Plateau. *Geophysical Journal International*, *162*(2), 575–590. https://doi.org/10.1111/j.1365-246X.2005.02580.x

Clark, M. K., & Royden, L. H. (2000). Topographic ooze: Building the eastern margin of Tibet by lower crustal flow. *Geology*, *28*(8), 703–706. https://doi.org/10.1130/0091-7613(2000)28%3C703:TOBTEM%3E2.0.CO;2

Copley, A. (2008). Kinematics and dynamics of the southeastern margin of the Tibetan Plateau. *Geophysical Journal International*, *174*(3), 1081–1100. https://doi.org/10.1111/j.1365-246X.2008.03853.x

Copley, A., Avouac, J.-P., & Wernicke, B. P. (2011). Evidence for mechanical coupling and strong Indian lower crust beneath southern Tibet. *Nature*, *472*(7341), 79–81. https://doi.org/10.1038/nature09926

Copley, A., & McKenzie, D. (2007). Models of crustal flow in the India–Asia collision zone. *Geophysical Journal International*, *169*(2), 683–698. https://doi.org/10.1111/j.1365-246X.2007.03343.x

Dziewonski, A., Chou, T. A., & Woodhouse, J. (1981). Determination of earthquake source parameters from waveform data for studies of global and regional seismicity. *Journal of Geophysical Research*, *86*(B4), 2825–2852. https://doi.org/10.1029/JB086iB04p02825

Ekström, G., Nettles, M., & Dziewoński, A. (2012). The global CMT project 2004–2010: Centroid-moment tensors for 13,017 earthquakes. *Physics of the Earth and Planetary Interiors*, *200*, 1–9.

England, P., & Molnar, P. (1997). Active deformation of Asia: From kinematics to dynamics. *Science*, *278*(5338), 647–650. https://doi.org/10.1126/science.278.5338.647

Fang, L., Wu, J., Zhang, T., Huang, J., Wang, C., & Yang, T. (2011). Relocation of mainshock and aftershocks of the 2011 Yingjiang Ms5. 8 earthquake in Yunnan (in Chinese with English abstract). *Acta Seismologica Sinica*, *33*(2), 262–267.

Fenton, C. H., Charusiri, P., & Wood, S. (2003). Recent paleoseismic investigations in Northern and Western Thailand. *Annals of Geophysics*, *46*(5), 957–981.

Gu, G., Lin, T., Shi, Z., & Li, Q. (1983). *Catalog of historic earthquakes in China (1831 BC–1969 AD)* (in Chinese with English Explantory Remarks). (pp. 894). Beijing: Science Press.

Gu, G., Lin, T., Shi, Z., & Wu, H. (1983). *Catalog of historic earthquakes in China (1970–1979 AD)* (in Chinese with English Explantory Remarks). Beijing: Science Press.

Guo, S.-M., Xu, X.-W., & Xiang, H.-F. (2002). Segmentation of earthquake rupture and earthquake prediction along the Longling-Lancang fault zone in the southwestern Yunnan Province. *Seismology and Geology*, *24*(2), 103–114.

Hall, R., & Morley, C. K. (2004). Sundaland Basins. In *Continent-ocean interactions within East Asian marginal seas* (pp. 55–85). Washington, DC: American Geophysical Union. https://doi.org/10.1029/149GM04

He, G.-W., Fu, B., Liu, M., Yang, S.-H., Shi, P., & Liu, F. (2014). Late-Quaternary deformation and geomorphic features along the Longing-Ruili fault (in Chinese with English abstract). *Seismology and Geology*, *36*(2), 434–448.

He, W.-G., Liu, X.-W., Yuan, D.-Y., Zhang, B., & Wu, M. (2015). Preliminary study on the Late Quaternary activity characteristics of the Menglian fault in southwest Yunnan (in Chinese with English abstract). *China Earthquake Engineering Journal*, *37*(4), 986–995.

Huang, X.-M., Du, Y., Shu, S.-B., & Xie, F.-R. (2010). Study of the late Quaternary slip rate along the northern segment on the south branch of Longling-Ruili fault (in Chinese with English abstract). *Seismology and Geology*, *32*(2), 222–232.

Huang, Z., Wang, L., Xu, M., Ding, Z., Wu, Y., Wang, P., et al. (2015). Teleseismic shear-wave splitting in SE Tibet: Insight into complex crust and upper-mantle deformation. *Earth and Planetary Science Letters*, *432*, 354–362. https://doi.org/10.1016/j.epsl.2015.10.027

Ji, L., Wang, Q., Xu, J., & Ji, C. (2017). The July 11, 1995 Myanmar–China earthquake: A representative event in the bookshelf faulting system of southeastern Asia observed from JERS-1 SAR images. *International Journal of Applied Earth Observation and Geoinformation*, *55*, 43–51. https://doi.org/10.1016/j.jag.2016.10.006

Kreemer, C., Blewitt, G., & Klein, E. C. (2014). A geodetic plate motion and global strain rate model. *Geochemistry, Geophysics, Geosystems*, *15*(10), 3849–3889. https://doi.org/10.1002/2014GC005407

Lacassin, R., Maluski, H., Leloup, P. H., Tapponnier, P., Hinthong, C., Siribhakdi, K., et al. (1997). Tertiary diachronic extrusion and deformation of western Indochina: Structural and 40Ar/39Ar evidence from NW Thailand. *Journal of Geophysical Research*, *102*(B5), 10,013–10,037. https://doi.org/10.1029/96JB03831

Lacassin, R., Replumaz, A., & Hervé Leloup, P. (1998). Hairpin river loops and slip-sense inversion on southeast Asian strike-slip faults. *Geology*, *26*(8), 703–706. https://doi.org/10.1130/0091-7613(1998)026%3C0703:hrlass%3E2.3.co;2

Lai, K.-Y., Chen, Y.-G., & Lâm, D. Đ. (2012). Pliocene-to-present morphotectonics of the Dien Bien Phu fault in northwest Vietnam. *Geomorphology*, *173-174*, 52–68. https://doi.org/10.1016/j.geomorph.2012.05.026

Lee, H.-Y., Chung, S.-L., & Yang, H.-M. (2016). Late Cenozoic volcanism in central Myanmar: Geochemical characteristics and geodynamic significance. *Lithos*, *245*, 174–190. https://doi.org/10.1016/j.lithos.2015.09.018

Lei, J., Zhang, G., Xie, F., Li, Y., Su, Y., Liu, L., et al. (2012). Relocation of the 10 March 2011 Yingjiang, China, earthquake sequence and its tectonic implications. *Earthquake Science*, *25*(1), 103–110. https://doi.org/10.1007/s11589-012-0836-4

Leloup, P. H., Harrison, T. M., Ryerson, F. J., Wenji, C., Qi, L., Tapponnier, P., & Lacassin, R. (1993). Structural, petrological and thermal evolution of a tertiary ductile strike-slip shear zone, Diancang Shan, Yunnan. *Journal of Geophysical Research*, *98*(B4), 6715–6743. https://doi.org/10.1029/92JB02791

Leloup, P. H., Lacassin, R., Tapponnier, P., Schärer, U., Zhong, D., Liu, X., et al. (1995). The Ailao Shan-Red River shear zone (Yunnan, China), Tertiary transform boundary of Indochina. *Tectonophysics*, *251*(1–4), 3–84. https://doi.org/10.1016/0040-1951(95)00070-4

Li, C., van der Hilst, R. D., Meltzer, A. S., & Engdahl, E. R. (2008). Subduction of the Indian lithosphere beneath the Tibetan Plateau and Burma. *Earth and Planetary Science Letters*, *274*(1–2), 157–168. https://doi.org/10.1016/j.epsl.2008.07.016

Li, S., Deng, C., Yao, H., Huang, S., Liu, C., He, H., et al. (2013). Magnetostratigraphy of the Dali Basin in Yunnan and implications for late Neogene rotation of the southeast margin of the Tibetan Plateau. *Journal of Geophysical Research: Solid Earth*, *118*, 791–807. https://doi.org/10.1002/jgrb.50129

Liang, S., Gan, W., Shen, C., Xiao, G., Liu, J., Chen, W., et al. (2013). Three-dimensional velocity field of present-day crustal motion of the Tibetan Plateau derived from GPS measurements. *Journal of Geophysical Research: Solid Earth*, *118*, 5722–5732. https://doi.org/10.1002/2013JB010503

Maurin, T., Masson, F., Rangin, C., Min, U. T., & Collard, P. (2010). First global positioning system results in northern Myanmar: Constant and localized slip rate along the Sagaing fault. *Geology*, *38*(7), 591–594. https://doi.org/10.1130/g30872.1

Molnar, P., England, P., & Martinod, J. (1993). Mantle dynamics, uplift of the Tibetan Plateau, and the Indian Monsoon. *Reviews of Geophysics*, *31*(4), 357–396. https://doi.org/10.1029/93RG02030

Molnar, P., & Lyon-Caen, H. (1988). Some simple physical aspects of the support, structure, and evolution of mountain belts. *Geological Society of America Special Papers*, *218*, 179–208. https://doi.org/10.1130/SPE218-p179

Molnar, P., & Lyon-Caen, H. (1989). Fault plane solutions of earthquakes and active tectonics of the Tibetan Plateau and its margins. *Geophysical Journal International*, *99*(1), 123–154. https://doi.org/10.1111/j.1365-246X.1989.tb02020.x

Nguyen, A. D., Sagiya, T., Kimata, F., To, T. D., Hai, V. Q., Cong, D. C., et al. (2013). Contemporary horizontal crustal movement estimation for northwestern Vietnam inferred from repeated GPS measurements. *Earth, Planets and Space*, *65*(12), 1399–1410.

Nualkhao, P., Charusiri, P., Sutiwanich, C., & Pailoplee, S. (2016). Paleoearthquakes along Xaignabouli Fault Zone in Western Lao PDR. *Bulletin of Earth Sciences of Thailand*, *7*(1), 25–32.

Pacheco, J. F., & Sykes, L. R. (1992). Seismic moment catalog of large shallow earthquakes, 1900 to 1989. *Bulletin of the Seismological Society of America*, *82*(3), 1306–1349.

Pailoplee, S., Channarong, P., & Chutakositkanon, V. (2013). Earthquake activities in the Thailand-Laos-Myanmar border region: A statistical approach. *Terrestrial, Atmospheric and Oceanic Sciences*, *24*(4-2), 721. https://doi.org/10.3319/TAO.2013.04.26.01(T)

Pananont, P., Herman, M. W., Pornsopin, P., Furlong, K. P., Habangkaem, S., Waldhauser, F., & Wechbunthung, B. (2017). Seismotectonics of the 2014 Chiang Rai, Thailand, earthquake sequence. *Journal of Geophysical Research: Solid Earth*, *122*, 6367–6388. https://doi.org/10.1002/2017JB014085

Pasyanos, M. E., Masters, T. G., Laske, G., & Ma, Z. (2014). LITHO1.0: An updated crust and lithospheric model of the Earth. *Journal of Geophysical Research: Solid Earth*, *119*, 2153–2173. https://doi.org/10.1002/2013JB010626

Penth, H. (2006). Earthquakes in Old Lan Na: A part of natural catastrophes. *Chiang Mai University Journal*, *5*(2), 255–265.

Replumaz, A., Lacassin, R., Tapponnier, P., & Leloup, P. (2001). Large river offsets and Plio-Quaternary dextral slip rate on the Red River fault (Yunnan, China). *Journal of Geophysical Research*, *106*(B1), 819–836. https://doi.org/10.1029/2000JB900135

Royden, L. H., Burchfiel, B. C., King, R. W., Wang, E., Chen, Z. L., Shen, F., & Liu, Y. P. (1997). Surface deformation and lower crustal flow in eastern Tibet. *Science*, *276*(5313), 788–790. https://doi.org/10.1126/science.276.5313.788

Royden, L. H., Burchfiel, B. C., & van der Hilst, R. D. (2008). The geological evolution of the Tibetan plateau. *Science*, *321*(5892), 1054–1058. https://doi.org/10.1126/science.1155371

Savage, J. C., & Burford, R. O. (1973). Geodetic determination of relative plate motion in Central California. *Journal of Geophysical Research*, *78*(5), 832–845. https://doi.org/10.1029/JB078i005p00832

Schoenbohm, L. M., Burchfiel, B. C., Liangzhong, C., & Jiyun, Y. (2006). Miocene to present activity along the Red River fault, China, in the context of continental extrusion, upper-crustal rotation, and lower-crustal flow. *Geological Society of America Bulletin*, *118*(5–6), 672–688. https://doi.org/10.1130/b25816.1

Shen, Z.-K., Lü, J., Wang, M., & Bürgmann, R. (2005). Contemporary crustal deformation around the southeast borderland of the Tibetan Plateau. *Journal of Geophysical Research*, *110*, B11409. https://doi.org/10.1029/2004JB003421

Shi, F. (2014). Tectonic geomorphology of the Nantinghe Fault in Southwestern Yunnan. PhD thesis (in Chinese with English abstract). Institute of Geology, China Earthquake Administration Beijing.

Shi, X., Kirby, E., Lu, H., Robinson, R., Furlong, K. P., & Wang, E. (2014). Holocene slip rate along the Gyaring Co Fault, central Tibet. *Geophysical Research Letters*, *41*, 5829–5837. https://doi.org/10.1002/2014GL060782

Simons, W. J. F., Socquet, A., Vigny, C., Ambrosius, B. A. C., Haji Abu, S., Promthong, C., et al. (2007). A decade of GPS in Southeast Asia: Resolving Sundaland motion and boundaries. *Journal of Geophysical Research*, *112*, B06420. https://doi.org/10.1029/2005JB003868

Sternai, P., Avouac, J.-P., Jolivet, L., Faccenna, C., Gerya, T., Becker, T. W., & Menant, A. (2016). On the influence of the asthenospheric flow on the tectonics and topography at a collision-subduction transition zones: Comparison with the eastern Tibetan margin. *Journal of Geodynamics*, *100*, 184–197. https://doi.org/10.1016/j.jog.2016.02.009

Sternai, P., Jolivet, L., Menant, A., & Gerya, T. (2014). Driving the upper plate surface deformation by slab rollback and mantle flow. *Earth and Planetary Science Letters*, *405*, 110–118. https://doi.org/10.1016/j.epsl.2014.08.023

Su, Z., Wang, E., Furlong, K. P., Shi, X., Wang, G., & Fan, C. (2011). Young, active conjugate strike–slip deformation in West Sichuan: Evidence for the stress–strain pattern of the southeastern Tibetan plateau. *International Geology Review*, *54*(9), 991–1012. https://doi.org/10.1080/00206814.2011.583491

Sun, H., He, H., Wei, Z., Shi, F., & Gao, W. (2017). Late Quaternary paleoearthquakes along the northern segment of the Nantinghe fault on the southeastern margin of the Tibetan Plateau. *Journal of Asian Earth Sciences*, *138*, 258–271. https://doi.org/10.1016/j.jseaes.2017.02.023

Tapponnier, P., Peltzer, G., & Armijo, R. (1986). On the mechanics of the collision between India and Asia. *Geological Society, London, Special Publications*, *19*(1), 113–157. https://doi.org/10.1144/GSL.SP.1986.019.01.07

Tapponnier, P., Peltzer, G., Le Dain, A. Y., Armijo, R., & Cobbold, P. (1982). Propagating extrusion tectonics in Asia: New insights from simple experiments with plasticine. *Geology*, *10*(12), 611–616. https://doi.org/10.1130/0091-7613(1982)10%3C611:PETIAN%3E2.0.CO;2

Tapponnier, P., Zhiqin, X., Roger, F., Meyer, B., Arnaud, N., Wittlinger, G., & Jingsui, Y. (2001). Oblique stepwise rise and growth of the Tibet Plateau. *Science*, *294*(5547), 1671–1677. https://doi.org/10.1126/science.105978

Taylor, M., & Yin, A. (2009). Active structures of the Himalayan-Tibetan orogen and their relationships to earthquake distribution, contemporary strain field, and Cenozoic volcanism. *Geosphere*, *5*(3), 199–214. https://doi.org/10.1130/ges00217.1

Tun, S. T., Wang, Y., Khaing, S. N., Thant, M., Htay, N., Htwe, Y. M. M., et al. (2014). Surface ruptures of the Mw 6.8 March 2011 Tarlay earthquake, Eastern Myanmar. *Bulletin of the Seismological Society of America*, *104*(6), 2915–2932. https://doi.org/10.1785/0120130321

Wang, C.-Y., Flesch, L. M., Chang, L., & Zheng, T. (2013). Evidence of active mantle flow beneath South China. *Geophysical Research Letters*, *40*, 5137–5141. https://doi.org/10.1002/grl.50987

Wang, E., & Burchfiel, B. (1997). Interpretation of Cenozoic tectonics in the right-lateral accommodation zone between the Ailao Shan shear zone and the eastern Himalayan syntaxis. *International Geology Review*, *39*(3), 191–219. https://doi.org/10.1080/00206819709465267

Wang, E., Burchfiel, B. C., Royden, L. H., Chen, L., Chen, J., Li, W., & Chen, Z. (1998). Late Cenozoic Xianshuihe-Xiaojiang, Red River, and Dali Fault Systems of Southwestern Sichuan and Central Yunnan, China. *Geological Society of America Special Papers*, *327*, 1–108. https://doi.org/10.1130/0-8137-2327-2.1

Wang, E., Kirby, E., Furlong, K. P., van Soest, M., Xu, G., Shi, X., et al. (2012). Two-phase growth of high topography in eastern Tibet during the Cenozoic. *Nature Geoscience*, *5*(9), 640–645. Retrieved from http://www.nature.com/ngeo/journal/v5/n9/abs/ngeo1538.html#supplementary-information, https://doi.org/10.1038/ngeo1538

Wang, G., Wan, J., Wang, E., Zheng, D., & Li, F. (2008). Late Cenozoic to recent transtensional deformation across the southern part of the Gaoligong shear zone between the Indian plate and SE margin of the Tibetan plateau and its tectonic origin. *Tectonophysics*, *460*(1-4), 1–20. https://doi.org/10.1016/j.tecto.2008.04.007

Wang, J.-H., Yin, A., Harrison, T. M., Grove, M., Zhang, Y.-Q., & Xie, G.-H. (2001). A tectonic model for Cenozoic igneous activities in the eastern Indo–Asian collision zone. *Earth and Planetary Science Letters*, *188*(1-2), 123–133. https://doi.org/10.1016/S0012-821X(01)00315-6

Wang, Y., Sieh, K., Tun, S. T., Lai, K. Y., & Myint, T. (2014). Active tectonics and earthquake potential of the Myanmar region. *Journal of Geophysical Research: Solid Earth*, *119*, 3767–3822. https://doi.org/10.1002/2013JB010762

Wang, Y., Wang, E., Shen, Z.-K., Wang, M., Gan, W., Qiao, X., et al. (2008). GPS-constrained inversion of present-day slip rates along major faults of the Sichuan-Yunnan region, China. *Science in China Series D: Earth Sciences*, *51*(9), 1267–1283. https://doi.org/10.1007/s11430-008-0106-4

Weldon, E., Weldon, R., Shi, X., Wiwegwin, W., & Owen, L. A. (2016). *The left-lateral Mae Chan fault, southern Shan Plateau, northern Thailand: New constraints on slip rate and recency of large earthquakes*. Paper presented at the Asia Oceania Geosciences Society Annual Meeting 2016, Beijing, China.

Weldon, R., Sieh, K., Zhu, C., Han, Y., Yang, J., & Robinson, S. W. (1994). *Slip rate and recurrence interval of earthquakes on the Hong He (Red River) fault, Yunnan, PRC*. Paper presented at the International Workshop on Seismotectonics and Seismic Hazard in South East Asia, Hanoi, Vietnam.

Wood, S. H. (2001). *Slip-rate estimate from offset streams, valley volumes, and denudation rate: Mae Chan Fault, Northern Thailand*. Paper presented at the AGU Fall Meeting Abstracts 2001, San Francisco.

Wu, Z.-H., Long, C.-X., Fan, T.-Y., Zhou, C., Feng, H., Yang, Z., & Tong, Y. (2015). The arc rotational-shear active tectonic system on the southeastern margin of Tibetan Plateau and its dynamic characteristics and mechanism (in Chinese with English abstract). *Geological Bulletin of China*, *34*(1), 1–31.

Xu, F., Liu, Z., Zhang, Z., Li, J., Liu, L., & Su, Y. (2015). Double difference relocation and focal mechanisms of the Jinggu Ms 6.6 earthquake sequences in Yunnan province in 2014 (in Chinese with English abstract). *EarthScienc-Journal of China University of Geosciences*, *40*(10), 1741–1754. https://doi.org/10.3799/dqkx.2015.156

Xu, X., Wen, X., Zheng, R., Ma, W., Song, F., & Yu, G. (2003). Pattern of latest tectonic motion and its dynamics for active blocks in Sichuan-Yunnan region, China. *Science in China Series D: Earth Sciences*, *46*(2), 210–226. https://doi.org/10.1360/03dz0017

Yang, T., Wu, J.-P., Fang, L.-H., & Wang, W.-L. (2016). Relocation of mainshock and aftershocks of the 2014 Yingjiang Ms 5.6 and Ms 6.1 earthquake in Yunnan. *Seismology and Geology*, *38*(4), 1047–1057.

Yao, H., van der Hilst, R. D., & Montagner, J.-P. (2010). Heterogeneity and anisotropy of the lithosphere of SE Tibet from surface wave array tomography. *Journal of Geophysical Research*, *115*, B12307. https://doi.org/10.1029/2009JB007142

Yin, A., & Taylor, M. H. (2011). Mechanics of V-shaped conjugate strike-slip faults and the corresponding continuum mode of continental deformation. *Geological Society of America Bulletin*, *123*(9–10), 1798–1821. https://doi.org/10.1130/B30159.1

Yu, W., Hou, X., Zhou, R., Chai, T., & Gu, Y. (1991). Characteristic surface ruptures of Lancang-Gengma earthquake (in Chinese with English abstract). *Journal of Seismological Research*, *14*(3), 203–214.

Zhang, S., & Liu, B. (1978). Seismic characteristicis of Tonghai earthquake in 1970 (in Chinese with English abstract). *Scientia Geologica Sinica*, (4), 323–335.

Zuchiewicz, W., Cuong, N. Q., Bluszcz, A., & Michalik, M. (2004). Quaternary sediments in the Dien Bien Phu fault zone, NW Vietnam: A record of young tectonic processes in the light of OSL-SAR dating results. *Geomorphology*, *60*(3-4), 269–302. https://doi.org/10.1016/j.geomorph.2003.08.004

Zuo, Z.-R., Zhang, G.-M., & Wu, J.-P. (1996). Analysis of the 1976 Longling, Yunnan, earthquake sequence of Ms 7.4 (in Chinese with English abstract). *Chinese Journal of Geophysics*, *39*(5), 653–659.